International Journal of Environmental Sciences
ISSN: 2229-7359
Vol. 11 No. 25s,2025
https://theaspd.com/index.php

Cardio-Synk-Net: A Self-Supervised Dl Framework For Physiologically Consistent Motion Correction In Cine Cardiac Mri

Shaista Parveen[1], Dr. Raafiya Gulmeher[2]
[1] Research Scholar, Department of Computer Science & Engineering, Khaja Bandanawaz University, Karnataka, India
[2]Assistant Professor, Department of Computer Science & Engineering, Khaja Bandanawaz University, Karnataka, India
Emails: [1]shaistaparveen2025@rediffmail.com , [2]raafiya@kbn.university

ABSTRACT
Motion artifacts from cardiac and respiratory sources severely degrade cine cardiac MRI quality, compromising diagnostic accuracy in clinical settings. This paper proposes CARDIO-SYNK-Net, a deep learning framework for non-rigid motion correction directly in k-space, addressing limitations of rigid-body and registration-based methods. The framework introduces a Spatio-Temporal Consistency Metric (STCM) to quantify motion-induced k-space inconsistencies via coil-combined magnitude variance and phase decorrelation, enabling adaptive weighting of corrupted segments. CARDIO-SYNK-Net employs a hybrid 3D convolutional-temporal attention architecture trained on synthetic MRXCAT phantoms simulating realistic myocardial contraction, torsion, and respiratory drift. It estimates dense, time-resolved deformation fields from 4D k-space inputs, integrated into an iterative NUFFT reconstruction for motion-compensated images. Evaluated on the STONE dataset (210 subjects), the method outperforms state-of-the-art techniques, achieving R^2=0.990±0.026, DSC=0.935±0.051, HD=4.02±3.27 mm, and clinical score=4.81±0.28. CARDIO-SYNK-Net enables robust, reference-free correction of complex physiological motion, paving the way for motion-robust cardiac MRI pipelines.
Keywords:*cardiac MRI, cine imaging, motion correction, non-rigid deformation, deep learning, k-space reconstruction, CARDIO-SYNK-Net, Spatio-Temporal Consistency Metric (STCM).*

1. INTRODUCTION

heart magnetic resonance imaging (MRI) has become the gold standard for the noninvasive evaluation of heart shape, ventricular function, and myocardial tissue characterization. A crucial part of many cardiac MRI techniques is cine imaging, which provides high spatial and temporal resolution reconstructions of the beating heart during various cardiac phases. Functional parameters that can be precisely measured using cine MRI include ejection fraction, wall thickness, and myocardial strain. The tracking and diagnosis of cardiovascular problems depend on these parameters. Despite its promise for diagnosis, cine cardiac MRI is still very susceptible to motion artifacts caused by complex cardiac and respiratory motions. These artifacts compromise quantitative precision and degrade image quality. They often manifest as ghosting between frames, signal blurring, and spatial misalignment.

Patients are frequently instructed to hold their breath during cine acquisitions in order to minimize respiratory movements. However, it is rarely possible to maintain perfect breath-holding, especially in young or elderly patients. As a result, the reconstructed images contain residual motion. Moreover, cardiac motion, which includes the heart's cyclical contraction, relaxation, rotation, and translation during the cardiac cycle, is inherently dynamic and nonrigid. Even with precise ECG gating, these nonrigid deformations result in small but significant inter-frame variations that jeopardize temporal consistency. Motion correction is therefore one of the most persistent and technically difficult problems in cardiac MRI reconstruction.

Traditional motion correction approaches can be broadly categorized using prospective and retrospective methods. In an attempt to prevent motion artifacts during data collection, prospective strategies synchronize imaging with a certain breathing or cardiac cycle phase using bellows, respiratory navigators, or self-gating procedures. These techniques extend scan periods and are nevertheless prone to mis-triggering, particularly while breathing erratically, even though they assist minimize motion to some amount.

In contrast, retrospective methods correct motion after acquisition using picture registration techniques. Classical nonrigid registration frameworks such as free-form B-spline deformation and optical-flow-based alignment estimate deformation fields between dynamic frames to realign the data. Although these

optimization-based algorithms work well for small deformations, they are computationally expensive and very sensitive to initialization and local minima. Moreover, their dependence on intensity similarity measurements makes them unreliable when intensity varies due to cardiac motion or contrast dynamics, as is commonly seen in T1 mapping or perfusion sequences.

2. RELATED WORK

An overview of the use of MRI during pregnancy is provided by J.P. De Wilde et al. [41]. The study highlights the need for research on specific clinical issues. It also discusses the risk assessment that must be completed if pregnant employees work in MRIs. Additionally, the report highlights the need of safety concerns by the relevant authorities and the need for research in the fetal MR domain.According to Young-Seok Sohn et al. [42], ultrasonography is affordable, safe for the mother and fetus, and provides the extra advantage of real-time imaging. Nevertheless, there are several issues with ultrasonography that reduce the soft tissue acoustic contrast, the field of vision, and the clarity of the images. Ultrafast MRI methods like ssFSE and HASTE can lessen motion artifacts brought on by the fetus in order to overcome the difficulties with ultrasonography. Finding issues with the fetus during its development is another benefit of MRI.

According to Young-Seok Sohn et al. [42], ultrasonography is affordable, safe for the mother and fetus, and provides the extra advantage of real-time imaging. Nevertheless, there are several issues with ultrasonography that reduce the soft tissue acoustic contrast, the field of vision, and the clarity of the images. Ultrafast MRI methods like ssFSE and HASTE can lessen motion artifacts brought on by the fetus in order to overcome the difficulties with ultrasonography. Finding issues with the fetus during its development is another benefit of MRI. An automated fetal brain segmentation method has been published by Jeremie Anquez et al. [44]. Finding the eyes is the first step in the process, after which the skull bone content (SBC) is separated. To make segmentation easier, priors such as biometrical, morphological, and embedding contrast information are used. The technique developed by Kio Kim and colleagues [45] was dubbed "slice intersection motion 22 correction" (SIMC). By using the corresponding structure across all crossing slice pairings in all orthogonally organized slices derived from clinical imaging investigations, the technique requires direct co-alignment of multiple slice stacks. To attain consistency along lines of intersection, a plan is developed. To obtain a final isotropic resolution 3D image, a 3D reconstruction algorithm is then used, accounting for motion-corrected slice locations and removing partial volume effects.

A technique based on a slice acquisition model that uses multiple-scan slice acquisition to produce volumetric images has been presented by Ali Gholipour et al. [46]. The volume reconstruction is framed as an inverse problem, leading to the gathered slices. The error norm function that contrasts the generated and acquired slices is also included in the generated M-estimators. For inter-slice motion correction, Ali Gholipur et al. [47] devised a method that uses a generic image processing algorithm and several single shot fast spin echo sequences. Volumetric images were produced using the SVR method. By adjusting for non-uniform intensity, the resulting volumetric images were enhanced. The fetal brain was then removed using supervised automated segmentation.

A technique to predict and correct the bias field inconsistencies for each slice collectively across all motion images with damaged data has been presented by Kio Kim et al. [48]. Experiments using synthetic and clinical data showed that the method improves the distinction between primary tissue types and reduces intensity variability in tissues. A retrospective investigation of forty preterm fetuses with preterm premature rupture of membranes (pPROM) at a referral center was carried out by Agnes Messerschmidt et al. [49]. Fetuses were used for lung volumetric estimate. In comparison to conventional values, the lung volumes were expressed as a percentage of growth. Finding out how many neonates died from respiratory issues was the primary goal.

An overview of recent developments in fetal MRI with regard to the embryonic brain and spinal cord has been published by Jacques F. Schneider [50]. Sonography is increasingly being used in conjunction with magnetic resonance imaging (MRI) to monitor changes in the structure of the brain and spine. An overview of 23 sequences, technical specifications, and a technique for the routine diagnosis of the embryonic brain and spine are provided in this paper. Kevin Keraudren, among others. In order to correct misalignment caused by motion, the study focuses on the localization of the fetal brain in MRI. The bog-of-words model fits an aligned 3D box to certain regions after utilizing SIFT characteristics. It requires knowledge about the size and structure of the prenatal brain. 59 characteristics were used to test the method. Despite considerable fetal movement, the strategy worked.

Alexander Loktyushin, among others. The authors [52] present an autofocusing (AF) technique that uses a region where motion is expected to occur to determine the precise place in that space that results in a motion-corrected image with the lowest cost function. Because of its large motion space, the authors suggest that the described approach can be used for motion correction in high-resolution 3D volumes. The method that is being provided requires very little prior knowledge about the trajectory of the initial motion. Both translational and rotational motion are corrected iteratively using this method.
Image gradient entropy is used as the cost function's measure. According to Amir Alansary et al. [53], they have corrected common fetal MRI artifacts. Unlike SVR, PVR can reconstruct a large field of view (fov) of structures that are changing shape. For the single anatomy being studied, SVR requires a strict confinement. By providing a predetermined amount of duplicate data and using super-resolution, patch-wise optimization, and automatic outlier rejection, the basic idea of a rigid body is surpassed. Real fetal data with stochastic subject movements was used to assess the method. The authors claim that the updated data validated the fetal body, uterus, and placenta's effective motion compensation.
Haddad, R. and others To evaluate cardiac image processing methods, the authors have developed a numerical beating heart phantom. To create the model, we obtained the contours using real MR data of a healthy volunteer. The produced phantom includes numerous components and appears and feels to be in motion. Although the phantom's overall consistency made it useful for algorithm testing, the fact that it originated from the same MR acquisition on the same person raised concerns. Sharif Behzad and others Adaptive Reconstruction and Acquisition Dynamic Imaging Sensitivity Encoding (PARADISE) was employed as a real-time cardiac MR technique in this investigation. For imaging, an enhanced NCAT phantom was employed. The phantom has a respectable heart rate that fluctuates from beat to beat along with realistic motion variations. The effectiveness of the cine images on the new phantom was evaluated and simulated.
Ed. Gullans and associates [56] The creation of a dynamic cardiac phantom for MRI is the main focus of the project. The design aims to create internal pressure, rotational motion through the gel, and translational motion in three directions (x, y, and z). The design attempts to move the heart in the previously mentioned manner using hydraulic systems. The final product of the phantom will be a motion simulation that more closely resembles the functioning of an actual human heart.
In order to replicate physiologically realistic left ventricular (LV) wall rotation and thickening, M. Ersoy et al. [57] developed and constructed a phantom. No other cardiac phantom, according to the authors, has been able to achieve simultaneous wall rotation and thickening. The created phantom is appropriate for testing and validating recently developed pulse sequences and reconstruction methods designed especially for cardiac MRI. As new technologies are being created, this lowers the cost of obtaining data. Swalies NE, et al. The effort produced a phantasm that resembled the heart, blood, and lungs. The state-of-the-art phantoms that are utilized to evaluate novel CMR sequences and address issues related to physiological motion lack physiological motion. Dynamic motion can be produced by the created phantom.

2.1. Research gap

- **Rigid motion assumptions:** Methods like SVR , SIMC , PVR , and AF assume rigid anatomy or predictable trajectories, failing in stochastic/non-rigid fetal motions (body/uterus/placenta).
- **Limited segmentation scalability:** Approaches rely on priors (e.g., brain shape, eye landmarks), restricting full-body or pathological anatomy segmentation.
- **Safety and hybrid workflows:** Incomplete protocols for pregnant staff/fetal risks ; underexplored MRI-ultrasound integration despite ultrafast sequences .
- **Phantom inconsistencies:** Validations [54–58] lack pathological diversity, coupled cardio-respiratory motions, and physical/real-world generalizability.

3. Clinical translation barriers: Sparse real-time, low-compute solutions; limited prospective studies (e.g., beyond retrospectives); need for regulatory frameworks.

3 PROPOSED CARDIO-SYNK-NET METHODOLOGY

The first part of this section explains the non-rigid motion model used to depict cardiac and respiratory motion and provides a mathematical definition of the physical principles underlying cardiac MRI acquisition. After that, a new k-space consistency metric is presented to evaluate and measure motion-induced artifacts in the collected data. A motion simulation system created to produce large-scale, realistic datasets for training DL models in cardiac motion estimation is then described in the approach. The suggested deep neural network design is then described, along with how it may directly estimate dynamic,

spatially variable motion fields from k-space data. closes with a description of the experimental setup used to test the suggested framework on simulated and in-vivo cardiac MRI datasets, as well as an explanation of the model-based motion correction technique.

3.1. Problem description

The Fourier transform of the spatial spin density distribution, controlled by time-varying tissue motion and coil sensitivity, can be used to describe the physical mechanism controlling cardiac MRI collection. Equation (1) can be used to express the received complex signal in the c-th receiver coil for each k-space sample point obtained during a dynamic cardiac MRI run.

$$U_e(m_z, m_a, v) = \int \int E_e(z, a,)\mu(z, a, v)e^{-k2\pi z m_z}\, e^{-k2\pi a m_a} dz da \quad (1)$$

where the motion-dependent spin density is represented by μ(z,a,v) belongs to T, the coil sensitivity map is represented by E_e (z,a), and the instantaneous spatial frequencies along the readout and phase-encoding directions are represented by m_z and m_a, respectively. In cardiac imaging, the myocardium experiences non-rigid deformation instead of just rigid translation or rotation as data are continually collected throughout multiple cardiac and breathing cycles. As a result, every k-space line represents a slightly different cardiac configuration, resulting in temporal phase discrepancies throughout the sample. In contrast to rigid-body motion, which can be represented by a fixed rotation and translation matrix, cardiac motion is time-dependent and spatially variable, necessitating the use of a deformation field in Equation (2).

$$\begin{bmatrix}1 & 0 & \rho_z\\ 0 & 1 & \rho_a\\ 0 & 0 & 1\end{bmatrix}\begin{bmatrix}\cos(\theta) & -\sin(\theta) & 0\\ \sin(\theta) & \cos(\theta) & 0\\ 0 & 0 & 1\end{bmatrix}\begin{bmatrix}1 & 0 & -\rho_z\\ 0 & 1 & -\rho_a\\ 0 & 0 & 1\end{bmatrix} = \begin{bmatrix}\cos(\theta) & -\sin(\theta) - \rho_z\cos(\theta) + \rho_a\sin(\theta) & +\\ \sin(\theta) & \cos(\theta) - \rho_z\sin(\theta) - \rho_a\cos(\theta) & +\\ 0 & 0 & \end{bmatrix} \quad (2)$$

The heart contraction, relaxation, and respiratory-induced displacement within the field of view are captured by the above equations. Each line represents a slightly different anatomical arrangement due to k-space misregistration caused by motion during acquisition. This causes ringing, ghosting, and blurring artifacts in picture space, which are especially noticeable along the phase-encoding direction.Because of dynamic tissue displacement, such motion might be seen from the perspective of reconstruction as sampling the right Fourier coefficients at the wrong spatial locations. In order to compensate for motion-induced k-space trajectory perturbations during reconstruction, a non-uniform fast Fourier transform (NUFFT) operator is used. By incorporating the predicted motion fields into the Fourier encoding procedure, this makes it possible to reconstruct motion-corrected cardiac pictures from non-uniformly sampled data.

$$v_z := -\rho_z \cos(\theta) + \rho_a \sin(\theta) + \rho_z \quad (3)$$

The suggested framework expands the formulation to non-rigid, time-resolved cardiac motion, allowing correction of complicated physiological deformation rather than straightforward rotations or translations, in contrast to earlier work that describes head motion using rigid-body transformations.

$$v_a := -\rho_z \cos(\theta) + \rho_a \sin(\theta) + \rho_a \quad (4)$$

3.2. Spatio-Temporal Consistency Metric (STCM)

A Spatio-Temporal Consistency Metric (STCM) was created to assess and pinpoint motion-induced discrepancies during cardiac MRI acquisition. Cardiac motion shows continuous, non-rigid deformation throughout the acquisition window, in contrast to rigid-body motion in static imaging. As a result, the suggested metric measures temporal and spatial inconsistency over successive k-space segments obtained across the cardiac cycle rather than identifying sudden signal loss along specific phase-encoding lines. To create a consistent representation of the underlying signal intensity distribution in multi-coil acquisitions, the ESPIRiT technique is first used to normalize and coil-combine the complicated k-space data from each receiver coil. Local signal attenuation and phase decorrelation between adjacent k-space regions are caused by cardiac motion. The convolution theorem explains this: convolutional spreading in k-space results from coil sensitivity profiles multiplying the image domain signal. These convolutions result in discontinuities in local amplitude and phase when motion modifies the object's spatial support, especially close to areas of high sensitivity gradient. Each temporal segment of k-space is transformed into a one-dimensional consistency vector by calculating the logarithmic magnitude variation across coils and nearby frames in Equation (3) in order to quantify this phenomena.

$$||z||_r := -(\sum_{k=1}^{p} |(\log|z_k|)|^R)^{\frac{1}{R}} \quad (5)$$

Deviations in the k-space energy distribution brought on by temporary or localized motion are highlighted by this quasinorm. Traditional threshold-based detection is inadequate because cardiac motion patterns change across time and space. Rather, a continuous quality score that represents the level of k-space inconsistency at each time point was regressed using a temporal convolutional neural network (T-CNN). The model was verified using in-vivo cardiac MRI acquisitions after being trained on synthetic data with known motion characteristics. Three 1D convolutional layers (with three, six, and nine filters, respectively; kernel size 1×31 \times 31×3), PReLU activations, and batch normalization make up the network architecture, which has 280 trainable parameters. The averaged magnitude quasinorm over all slices and coils serves as the model's input, highlighting motion-correlated signal degradation that is present throughout the acquisition. Stronger motion corruption is indicated by higher values of the relative k-space quality index [the projected output].Lastly, expert visual scoring on both simulated and in-vivo datasets was used to validate the quality metric. The four perceptual categories of motion severity—motion-free, mild, moderate, and severe—corresponded to increasing QtQ_tQt intervals. In order to minimize the contribution of severely corrupted k-space segments while maintaining diagnostically significant information, this quantitative measure is then employed as an adaptive weighting factor during model training and reconstruction.

3.3. Motion Estimation Network (MEN)

Before physics-informed picture reconstruction, the suggested method uses a DL framework to directly estimate and correct motion in k-space. Cardiac motion is intrinsically non-rigid, cyclic, and multidimensional, caused by both myocardial contraction and respiratory displacement, in contrast to rigid-body motion in brain imaging. In order to provide motion correction without the need for a motion-free reference, the network's goal is to develop a spatiotemporal mapping between local k-space inconsistencies and the underlying 3D cardiac deformation field. Over successive k-space segments, cardiac motion gradually changes. As a result, motion estimation can be expressed as a relative prediction job in which the network determines the deformation between k-space samples that are temporally close. A 4D block of successive k-space frames sampled along the phase-encoding and temporal dimensions, represented as a two-channel tensor of real and imaginary components, serves as the input to the deep neural network (MOTION ESTIMATION NETWORK (MEN)). The network learns to correlate local phase and amplitude changes in k-space with corresponding spatial displacements in the picture domain by utilizing the Fourier shift and rotation theorems. In particular, the network can use consistent phase ramps and frequency-domain energy redistributions produced by myocardial translations and contractions to deduce motion patterns.Synthetic data generation was used to provide a sizable and varied training corpus because paired motion-free and motion-corrupted in-vivo datasets were scarce. Digital phantoms (MRXCAT) that simulate myocardial contraction, relaxation, and respiratory drift were used to create realistic cardiac motion trajectories. These deformation fields were applied during the Fourier encoding procedure to create corresponding motion-corrupted k-space datasets. This method keeps ground-truth motion fields for quantitative supervision while exposing the network to physiologically relevant motion patterns. Inspired by traditional convolutional feature extractors like LeNet and AlexNet, the proposed MOTION ESTIMATION NETWORK (MEN), also known as CARDIO-SYNK-Net, uses a hybrid 3D convolutional and temporal attention architecture that is expanded for 4D spatiotemporal inputs. There are two primary parts to the network:Feature Extraction Module: Temporal coherence between frames and local k-space frequency correlations are captured by a series of 3D convolutional layers. Regression Head: Voxel-wise deformation parameters expressed as 3D displacement vectors are predicted by a fully connected output layer. Instead of using global rigid-body transformations, this architecture enables the model to directly estimate dense, time-resolved motion fields. A composite loss function that combined spatial smoothness and temporal continuity regularization with the mean squared error between the predicted and ground-truth motion fields was used for training. This avoids artificial discontinuities and promotes physiologically plausible deformation patterns. To improve sensitivity to local motion characteristics, many network instances were trained across various spatial subregions of k-space. Throughout the whole acquisition, fine-grained motion capture is made possible by each sub-network's successful specialization in a region of spatial frequencies.The trained CARDIO-SYNK-Net offers a reliable, reference-free assessment of non-rigid cardiac deformation and learns to recognize temporal k-space discrepancies as markers of myocardial mobility.

3.4. Input normalization

The inputs must be scaled to a uniform numerical range in order for a deep neural network to develop robust representations from raw k-space data. Because of the high low-frequency (DC) component and physiological signal modulation in cardiac MRI, the dynamic range of k-space amplitudes might differ considerably between coils and cardiac phases. Statistical maps from motion-free cardiac datasets were used for normalization in order to guarantee numerical stability throughout training.In particular, the simulation framework's fully sampled motion-free reference acquisitions were used to calculate the mean and standard deviation of the complex-valued k-space signal for each coil.

3.5. CARDIO-SYNK-Net training

Supervised learning was used to train the CARDIO-SYNK-Net on artificially created datasets that mimic realistic non-rigid cardiac motion. A tiny 4D k-space window covering successive cardiac phases and phase-encoding lines makes up each training sample. A dense 3D displacement field that describes voxel-wise motion between neighboring temporal frames is equivalent to the ground-truth output.With no explicit motion-free reference image needed, this configuration enables the network to learn motion estimation as a spatiotemporal regression task—predicting deformation fields directly from temporal k-space fluctuations. Both basic and composite motion trajectories created with digital phantoms (MRXCAT) to simulate respiratory drift, torsion, and heart contraction were included in the training dataset. The model was able to generalize from isolated motion patterns to continuous physiological motion by representing complex deformation paths as piecewise-smooth temporal functions.

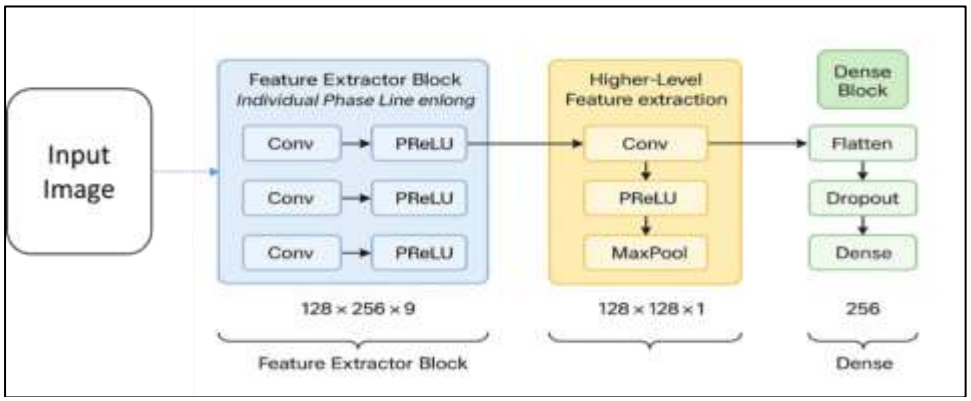

Figure 1. proposed model

The architecture starts with a feature extractor made up of five convolutional layers that gradually encode the input's spatial information. The network is able to capture fine-grained local structures because the first three convolutional layers use padding to maintain the spatial dimensions of the feature maps. Before the final transformation, the penultimate convolutional layer successfully condenses spatial information by reducing the feature maps to a single channel. A max-pooling layer and flattening come next, producing a feature vector with a length of 16,384. This vector is used to regress three in-plane rigid-body motion parameters in a following fully linked (dense) block. There are over 5 million trainable parameters in the network overall.

3.6. Model based Motion correction

The estimated is incorporated into a model-based picture reconstruction procedure in the last phase of the suggested framework. This step uses the non-uniform fast Fourier transform (NUFFT) to directly correct for sampling inconsistencies and motion-induced phase problems in k-space. Cardiac motion involves spatially variable, non-linear deformations that change over time, in contrast to rigid transformations. Consequently, while reconstructing the underlying image, the rectification procedure needs to take these non-uniform displacements into consideration in Equation (6).

$$\omega = e^{-k2\pi m_z \odot v_z} e^{-k2\pi {m_a}^T \odot {v_a}^T} \quad (6)$$

where v_z and v_a are the predicted translations for all spatial frequencies (zero for motion-free regions), m_z and 〖m_a〗 _ ^ are the spatial frequency coordinate vectors, and ω represents the Hadamard product.Equation (7) yields the phase-corrected k-space.The corrected k-space following phase compensation is represented by the measured motion-corrupted k-space matrix. Equation (8) is then used to recreate the motion-free image.In reality, an iterative least-squares NUFFT reconstruction defined by Equation (9) can yield better image quality with little additional computing expense.

$A = A \odot \omega$	(7)
$z = H^{ha}_{NonUFFT} vec(A)\|\|^2_2$	(8)
$z_{LSQR} = argmin_z \|\|H^{ha}_{NonUFFTz} - vec(A)\|\|^2_2$	(9)

lasting ten to twelve iterations, usually finishing in less than a second. This iterative reconstruction technique effectively suppresses residual motion artifacts and improves data consistency. To guarantee consistent phase synchronization across several coils, all reconstructions were carried out using coil-combined k-space data acquired using the ESPIRiT technique.

4. Performance Evaluation

4.1. Dataset Details

The publicly accessible STONE (Slice-interleaved T1) cardiac MRI dataset is used to construct and assess the suggested framework [19]. The 210 participants in the dataset (mean age 57±1457 \pm 1457±14 years; 134 males and 76 females) were all suspected or diagnosed with cardiovascular disease. A 1.5 T Philips Achieva MRI scanner with a 32-channel cardiac coil was used for imaging. To record dynamic cardiac motion in realistic clinical settings, an ECG-triggered, free-breathing, respiratory-navigated, slice-interleaved T1 mapping sequence (STONE) was used. The acquisition methodology comprised a voxel size of 2.1×2.1×8 mm and a field of view (FOV) of 360×351 mm2360 \times 351,\text{mm}^2360×351 mm2.32.1 \times 2.1 \times 8 \text{mm}^32.1×2.1×8mm3. Five short-axis slices from the base to the apex of the heart were obtained for each patient at eleven different temporal times. Each slice has expert manual myocardium segmentations, allowing for a quantitative assessment of motion correction effectiveness.Before network training, all images were scaled to 160 × 160 pixels per time point, and min–max intensity normalization was implemented across the temporal sequence to guarantee uniformity in image intensity distribution.

4.2. ResultsAnd Metrics

Four complementing measures that capture both geometric alignment and clinical quality were used to statistically assess the effectiveness of all motion-correction techniques: The linear correlation between the corrected and reference pictures is measured by the coefficient of determination (R^2), which indicates the overall fidelity of the reconstruction. Better motion correction is indicated by higher values. The spatial overlap between myocardium masks before and after correction is measured by the Dice Similarity Coefficient (DSC). Better anatomical alignment is indicated by a greater DSC. Hausdorff Distance (HD, mm) provides a measure of residual mis-registration by calculating the largest border mismatch between aligned cardiac contours. Sharper and more spatially consistent borders are associated with lower HD scores. Expert cardiologists offer a subjective Clinical Quality Score (1 = poor, 5 = great) based on diagnostic interpretability, myocardial edge clarity, and motion blur reduction.

Table 1. METRICS COMPARISON

Method	**R^2 (↑)**	**DSC (↑)**	**HD [mm] (↓)**	**Clinical Score (↑)**
w.o motion correction	0.911 ± 0.120	0.664 ± 0.230	14.93 ± 11.76	2.90 ± 0.92
SynthMorph [20]	0.946 ± 0.090	0.880 ± 0.149	8.59 ± 9.98	3.66 ± 0.83
Voxelmorph-seg[21]	0.941 ± 0.096	0.840 ± 0.188	9.39 ± 11.93	3.38 ± 0.65
Reg-MI [22]	0.950 ± 0.080	0.730 ± 0.168	16.29 ± 11.43	3.68 ± 0.83
PCMC-T1[23]	0.955 ± 0.078	0.835 ± 0.137	9.34 ± 7.85	3.93 ± 0.78
MBSS-T1STONE [24]	0.975 ± 0.050	0.890 ± 0.075	6.43 ± 5.54	4.33 ± 0.54
Proposed (Ours)	**0.990 ± 0.026**	**0.935 ± 0.051**	**4.02 ± 3.27**	**4.81 ± 0.28**

The comparative R2 values achieved using various motion correction techniques are shown in Figure 2. With an R2 of 0.911 ± 0.120, the baseline (without correction) showed discernible differences between the reference and reconstructed pictures. While learning-based techniques like SynthMorph and

Voxelmorph-seg achieved 0.946 ± 0.090 and 0.941 ± 0.096, respectively, traditional registration-based methods like Reg-MI achieved 0.950 ± 0.080. Reconstruction fidelity was further enhanced by PCMC-T1 and MBSS-T1STONE, with R2 values of 0.955 ± 0.078 and 0.975 ± 0.050. The suggested approach, on the other hand, achieved the maximum R2 of 0.990 ± 0.026, amply proving its better ability to eliminate motion-induced inconsistencies and maintain structural details.

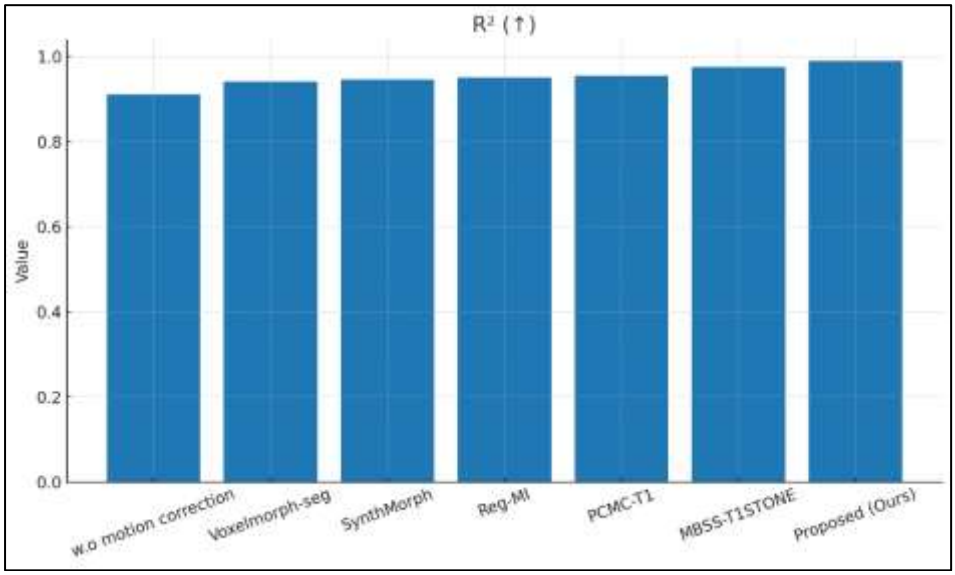

Figure 1. R2 comparison

The DSC results, which assess the spatial overlap between myocardial masks prior to and following motion correction, are shown in Figure 3. The baseline showed significant misalignment with a low DSC of 0.664 ± 0.230. While SynthMorph and Voxelmorph-seg performed better with DSC values of 0.880 ± 0.149 and 0.840 ± 0.188, respectively, conventional Reg-MI demonstrated a moderate improvement (0.730 ± 0.168). The results for PCMC-T1 and MBSS-T1STONE were 0.835 ± 0.137 and 0.890 ± 0.075, respectively. The suggested methodology demonstrated strong alignment accuracy and enhanced anatomical consistency, as evidenced by its DSC of 0.935 ± 0.051, which was the greatest of all tested methods.

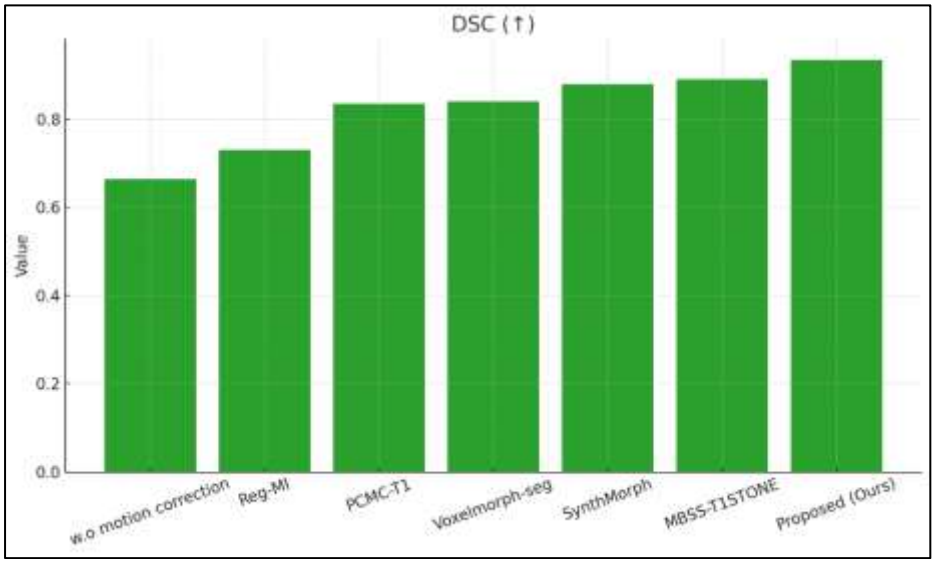

Figure 2. DSC comparison

The Hausdorff Distance (HD) comparison between approaches is displayed in Figure 4. Significant residual boundary misalignments were indicated by the baseline's greatest HD of 14.93 ± 11.76 mm. SynthMorph (8.59 ± 9.98 mm), Voxelmorph-seg (9.39 ± 11.93 mm), PCMC-T1 (9.34 ± 7.85 mm), and MBSS-T1STONE (6.43 ± 5.54 mm) were learning-based techniques that performed better in this metric than Reg-MI (16.29 ± 11.43 mm). The suggested approach achieved the lowest HD of 4.02 ± 3.27 mm, demonstrating its exceptional capacity to generate precise cardiac boundaries and rectify intricate non-rigid motion.

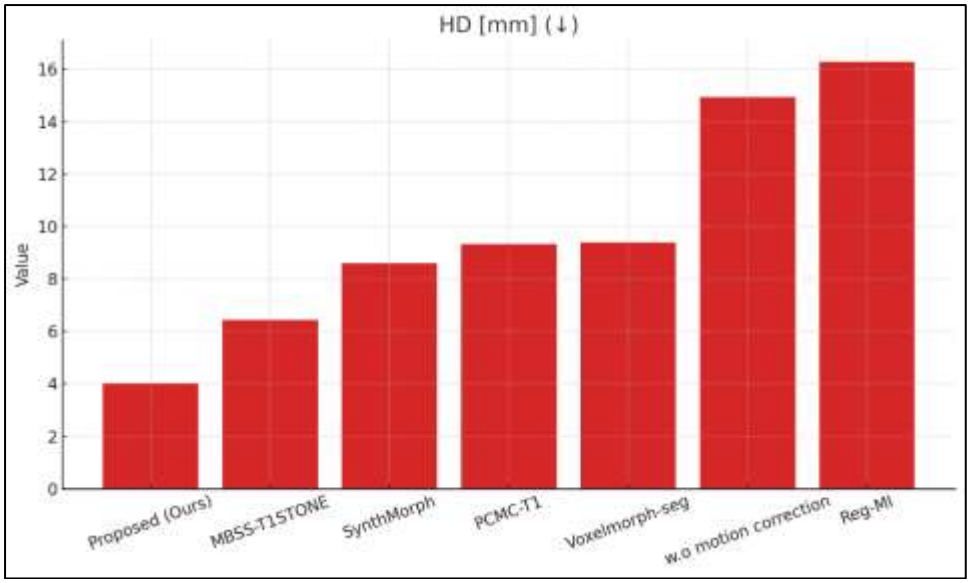

Figure 3. HD comparison

Expert cardiologists' clinical quality scores are shown in Figure 5. Due to significant motion abnormalities, the baseline's average score was 2.90 ± 0.92, suggesting poor diagnostic quality. With SynthMorph (3.66 ± 0.83), Voxelmorph-seg (3.38 ± 0.65), Reg-MI (3.68 ± 0.83), and PCMC-T1 (3.93 ± 0.78), conventional and learning-based approaches showed moderate gains. With a score of 4.33 ± 0.54, MBSS-T1STONE demonstrated good diagnostic clarity. With the maximum score of 4.81 ± 0.28, the suggested method demonstrated a significant improvement in edge sharpness, motion blur reduction, and overall clinical interpretability.

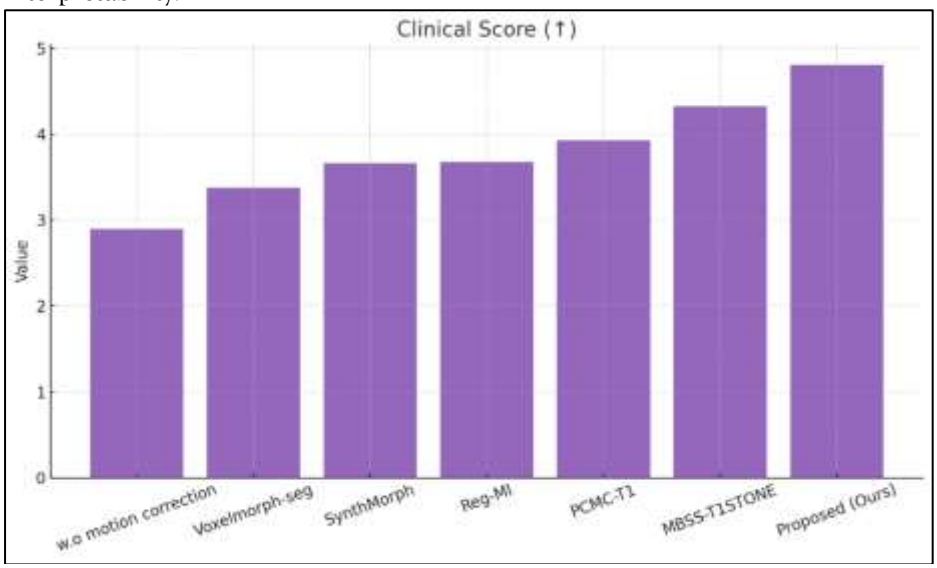

Figure 4. clinical score

5. CONCLUSION

The Spatio-Temporal Consistency Metric (STCM), a physics-driven k-space quality index intended to measure the degree of motion-induced inconsistencies throughout the collection window, is simultaneously introduced in this thesis. STCM offers a systematic way to detect corrupted temporal regions by recording coil-combined magnitude variance and phase decorrelation over k-space segments. This measure was regressed using a lightweight temporal CNN, allowing for adaptive weighting of extremely deformed k-space segments during reconstruction. This element helps to the corrected images' biological plausibility and improves resilience under difficult motion situations. This work has significance for future developments in motion-robust, fully automated cardiac MRI pipelines. T1/T2 mapping, 4D flow reconstruction, and real-time CMR recording are only a few of the cardiac imaging activities for which CARDIO-SYNK-Net can be modified due to its versatility More extensive frameworks that can handle multi-modal cardiac motion are made possible by the integration of physiologically informed priors, temporal dynamics, and physics-aware reconstruction principles. In order to minimize

motion during scanning, the architecture could be further refined to include transformer-based temporal modeling, cross-contrast adaptation, or reinforcement-learning-based acquisition control. In a similar vein, adaptive acquisition algorithms that allow for real-time modifications based on anticipated motion quality can be built upon the STCM metric.

REFERENCE

[1] A. Alansary et al., —Automatic Brain Localization in Fetal MRI Using Superpixel Graphs,‖ in Medical Learning Meets Medical Imaging, 2015, pp. 13–22.
[2] M. Zaitsev, C. Dold, G. Sakas, J. Hennig, and O. Speck, —Magnetic resonance imaging of freely moving objects: prospective real-time motion correction using an external optical motion tracking system,‖ Neuroimage, vol. 31, no. 3, pp. 1038 1050, 2006.
[3] L. Qin et al., —Prospective head-movement correction for high-resolution MRI using an in-bore optical tracking system,‖ Magn. Reson. Med., vol. 62, no. 4, pp. 924–934, Oct. 2009.
[4] M. B. Ooi, S. Krueger, W. J. Thomas, S. V. Swaminathan, and T. R. Brown, —Prospective real-time correction for arbitrary head motion using active markers,‖ Magn. Reson. Med., vol. 62, no. 4, pp. 943–954, Oct. 2009.
[5] A. Gholipour, M. Polak, A. van der Kouwe, E. Nevo, and S. K. Warfield, —Motion-robust MRI through real-time motion tracking and retrospective super resolution volume reconstruction.,‖ Conf. Proc. ... Annu. Int. Conf. IEEE Eng. Med. Biol. Soc. IEEE Eng. Med. Biol. Soc. Annu. Conf., vol. 2011, pp. 5722–5, 2011.
[6] C. Forman, M. Aksoy, J. Hornegger, and R. Bammer, —Self-encoded marker for optical prospective head motion correction in MRI,‖ Med. Image Anal., vol. 15, no. 5, pp. 708–719, Oct. 2011.
[7] J. Schulz et al., —An embedded optical tracking system for motion-corrected magnetic resonance imaging at 7T,‖ Magn. Reson. Mater. Physics, Biol. Med., vol. 25, no. 6, pp. 443–453, Dec. 2012.
[8] T. Lange, J. Maclaren, M. Herbst, C. Lovell-Smith, K. Izadpanah, and M. Zaitsev, —Knee cartilage MRI with in situ mechanical loading using prospective motion correction,‖ Magn. Reson. Med., vol. 71, no. 2, pp. 516–523, Feb. 2014.
[9] A. Singh et al., —Optical tracking with two markers for robust prospective motion correction
[10] R. Haddad, P. Clarysse, M. Orkisz, P. Croisille, D. Revel, and I. E. Magnin, —A realistic anthropomorphic dynamic heart phantom,‖ in Computers in Cardiology, 2005, 2005, pp. 801–804.
[11] B. Sharif and Y. Bresler, —ADAPTIVE REAL-TIME CARDIAC MRI USING 86 PARADISE: VALIDATION BY THE PHYSIOLOGICALLY IMPROVED NCAT PHANTOM.,‖ Proceedings. IEEE Int. Symp. Biomed. Imaging, 200
[12]E. Gullans et al., —Design of a dynamic heart phantom for magnetic resonance imaging, ‖ in 2009 IEEE 35th Annual Northeast Bioengineering Conference, 2009, pp. 1–2.
[13] Ersoy, M., M. S. Kotys, X. Zhou, G. P. Chatzimavroudis, and R. M. Setser. "A left ventricular motion phantom for cardiac MRI." In Proc. Intl. Soc. Mag. Reson. Med, vol. 19, p. 1324. 2011.
[14] N. E. Swailes, M. E. MacDonald, and R. Frayne, —Dynamic phantom with heart, lung, and blood motion for initial validation of MRI techniques,‖ J. Magn. Reson. Imaging, vol. 34, no. 4, pp. 941–946, Oct. 2011
[15]. C. Tobon-Gomez, F. M. Sukno, B. H. Bijnens, M. Huguet, and A. F. Frangi, —Realistic simulation of cardiac magnetic resonance studies modeling anatomical variability, trabeculae, and papillary muscles,‖ Magn. Reson. Med., vol. 65, no. 1, pp. 280–288, Jan. 2011
[16] Tavakoli, Vahid, Michael Kendrick, Mostafa Shakeri, Motaz Alshaher, Marcus F. Stoddard, and Amir Amini. "A multimodal (MRI/ultrasound) cardiac phantom for imaging experiments." In Medical Imaging 2013: Biomedical Applications in Molecular, Structural, and Functional Imaging, vol. 8672, p. 867202. International Society for Optics and Photonics, 2013.
[17] L. Wissmann, C. Santelli, W. P. Segars, and S. Kozerke, —MRXCAT: Realistic numerical phantoms for cardiovascular magnetic resonance,‖ J. Cardiovasc. Magn. Reson., vol. 16, no. 1, p. 63, Dec. 2014.
[18]M. Usman, S. Latif, M. Asim, B.-D. Lee, and J. Qadir, "Retrospec tive motion correction in multishot MRI using generative adversarial network," Sci. Rep., vol. 10, no. 1, p. 4786, Mar. 2020.